Strength and stiffness of adhesively bonded timber-steel composite beams

Simon Aurand[1], Peter Haase[2], Jakob Boretzki[2], Matthias Albiez[2], Philipp Dietsch[1], Thomas Ummenhofer[2]

[1] KIT Timber Structures and Building Construction, Karlsruhe

[2] KIT Steel and Lightweight Structures, Karlsruhe

Keywords: timber, steel, adhesive bonding, timber-steel composite

1 Introduction

1.1 Background

As a sustainable building material, timber can help replace conventional CO_2-intensive construction materials. To further establish timber structures in the sector of e.g. office buildings, appropriate cross-sections for large spans are required. These could be realized as composite cross-sections consisting of different materials. The materials timber and steel can complement each other in composite cross-sections and compensate for the weaknesses of the other bonding partner (*Riola Parada* (2016)). Advantages include the use of slender steel profiles, as they are embedded in the timber and local stability failure is prevented. Also, the fire resistance is increased by the embedment in the timber. Finally, the composite beams allow for typical bolted steel connections with high load-carrying capacity and stiffness, as is usual in steel construction.

1.2 State of the art

Numerous research projects have studied the potential of composite timber beams by adding a composite partner horizontally either in the tensile zone (of bending beams) or in both, the tensile and compressive zone. *Blaß & Romani* (2000) and *Blaß et al.* (2003) adhesively bonded carbon-fibre-reinforced polymers (CFRP) to GLT beams and performed 4-point bending tests. The area ratio of CFRP to timber was merely 0.4 to 3.0%. They determined an increase of 25 to 100% in load-carrying capacity and of 10 to 110% in bending stiffness. The test data showed that a significant increase in bending stiffness of ≥100% was only possible with the highest tested area ratio of 3.0%. *Shekarchi et al.* (2020) adhesively bonded pultruded GFRP profiles to timber beams. The results showed an increase of the bending stiffness of only 20 to 60%, although the area ratios were quite high with 5% to 17%. In these, the moduli of elasticity (*MOE*) of the used materials were almost equal, with a ratio (E_{Timber}/E_{GFRP}) of 0.77. *Fukutomi &*

Shioya (2018) and *Mori & Shioya* (2021) adhesively bonded steel rebars in the tensile and compressive zone of timber beams, and also performed 4-point bending tests. The results are quite promising, with an increase in load-carrying capacity of 25 to 100% and a significant increase in bending stiffness of 130 to 280%. The higher increases (180 to 280%) are due to an area ratio of 3.6 to 11%, a ratio of the *MOE*s (E_{Timber}/E_{Steel}) of approx. 0.05, and a ratio of timber bending strength to steel tensile strength of approx. 0.15.

The following research projects inserted a flatwise arranged joining partner in horizontal orientation: *Alam* (2004) investigated internally reinforced LVL, by joining steel and LVL either with nails or adhesive bonding. The evaluation of the results showed an increase in load-carrying capacity of max. 50% and an increase of bending stiffness of 170% (both for the adhesively bonded specimens). *Riola Parada* (2016) embedded steel I-profiles in GLT and CLT and joined the hybrid partners with bolts. The tests showed an increase in bending stiffness of 50%, when the profile was arranged symmetrically, and of 110%, when the profile was arranged asymmetrically. For both research projects with vertically arranged steel profiles, the area ratio (A_{steel}/A_{timber}), the ratio of the *MOE*s (E_{timber}/E_{steel}), and the ratio of bending to tensile strength (f_m/f_u) were quite similar, with values of approx. 0.05, 0.06, and 0.12, respectively.

Concluding from the evaluation of the cited literature it can be stated that the area ratio of the two joined materials needs to be high enough (>0.03). The ratio of the *MOE*s, however, needs to be low enough (approx. 0.05), while on the other side, the ratio of bending to tensile strength should not be too low (>0.05) whilst simultaneously not too high either (<0.3). Furthermore, the bond between the two composite partners has to be sufficient. This is highlighted by the results of the vertical reinforcement, where the ratios all fit the aforementioned requirements, but the max. increase in stiffness was still 100%. Here, the bond was realized with nails or bolts and did, therefore, not have sufficient stiffness. Table 1 summarises the evaluated results from the cited literature and the corresponding ratios of the specimens' properties.

Table 1. Results from literature: increase in load-carrying capacity F_{max}; increase in bending stiffness EI; area ratio of joined material 1 to timber; ratio of MOE of timber to material 1; ratio of bending to tensile strength of timber to material 1.

		Mat.	ΔF_{max}	ΔEI	Area ratio	Ratio *MOE*	Ratio f_m/f_u
Horizontal	*Blaß & Romani* (2000)	CFRP	25–100%	10–110%	0.4–3.1%	7–16%	1.5–4.6%
	Blaß et al. (2003)	CFRP	40–75%	10–35%	0.4–0.9%	6–15%	1.5–3.5%
	Shekarchi et al. (2020)	GFRP	-	20–60%	5.0–17%	77%	29%
	Fukutomi & Shioya (2018)	Steel	25-95%	130–280%	2.6–11%	4%	15%
	Mori & Shioya (2021)	Steel	-	180–250%	3.6–5.5%	4%	14%
Vertical	*Alam* (2004)	Steel	50%	70*–170%	5.4%	6%	12%
	Riola Parada (2016)	Steel	-	50–100%	4.6–5.4%	6%	13%

* nailed specimens

To investigate the bond of different state of the art and recently developed joining techniques, *Haase et al.* (2024a) conducted small-scale tensile tests on double-shear, steel-to-timber specimens with dowel-type fasteners, punched metal plate fasteners (PMPF), and adhesive bonds. The results demonstrated that the stiffness of the adhesively bonded specimens was 93 times higher than that of the dowel-type fasteners, and 5.5 times higher than that of the PMPFs.

1.3 Objective and investigated geometries

The aim of the research project was to develop, systematically investigate, and optimize the structural design of timber-steel composite beams. Specifically, the project sought to achieve the following scientific and technical research results: selecting and characterizing suitable wood and steel materials and profile cross-sections; designing and optimizing suitable timber-steel composite cross-sections and their manufacturing processes; experimentally investigating the composite load-carrying and failure behaviour using different composite methods; experimentally investigating the bending and shear load-carrying capacity, resistance, and long-term load-carrying behaviour of composite timber-steel beams; and developing a near-standard design model for designing the composite cross-sections.

This paper is an excerpt of the research project and contains the experimental investigations determining the load-carrying capacity and stiffness under governing bending and shear load.

The investigated geometries included Glulam GL 24h reference beams, laminated veneer lumber LVL 48p reference beams, and composite beams with two different geometry combinations (see Figure 1.1) and two different material combinations. A combination of steel S355 and GL 24h was analysed for both geometry variants (regular strength – RS). Additionally, steel S420 was tested in the vertical geometry in combination with LVL 48p and the horizontal geometry with beech LVL 80p (higher strength – HS). This paper summarises the results of the 4-point bending tests, which are fully detailed in *Haase et al.* (2024b), and supplements these with the results of the 3-point bending tests. The experimentally determined load-carrying capacities and stiffness values are compared with analytically determined values.
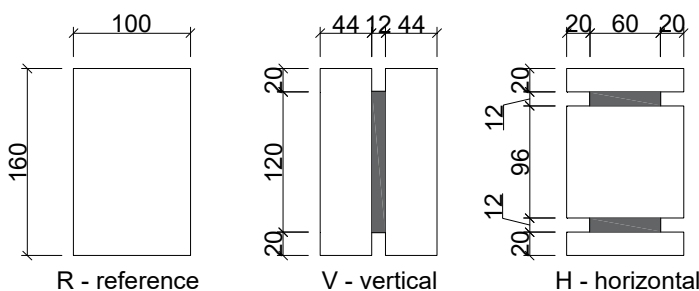

Figure 1.1. Geometries of tested specimens for all material combinations (all dimensions in mm).

2 Materials and methods

2.1 Materials

2.1.1 Timber and steel

The specimens analysed were made of glulam GL 24h, softwood LVL 48p and beech LVL 80p (BauBuche). The mechanical properties bending strength f_m, shear strength f_v and *MOE* of GL 24h and LVL 48p were determined according to EN 408 (2010). The mechanical properties of LVL 80p were taken from the LVL Handbook Europe (2020). A coefficient of variation of 5% was assumed for LVL 80p, to convert the characteristic values to mean values. For the steel plates, two steel grades were used, i.e. a mild steel S355 and higher strength steel S420. The ratio of *MOE* of timber to steel was 5.3% for GL 24h, 6.0% for LVL 48p, and 8.0% for LVL 80p. Tensile tests were performed to determine the yield and tensile strength of the steel plates in accordance with EN ISO 6892-1 (2020). The ratio of the bending strength f_m of the timber to the tensile strength f_u of the steel was 6.6% for GL 24h+S355, 10% for LVL 48p+S420 and 17% for LVL 80p+S420. All material properties are given in Table 2.

2.1.2 Adhesives

Three different adhesives were used to bond timber and steel. Two two-component epoxy adhesives (EP1 and EP2), and a polyurethane (PUR) system were compared. The material values of EP1 were determined in *Grunwald et al.* (2019). Tensile tests according to EN ISO 527-2 (2012) were performed to determine the material properties of the EP2 and PUR adhesives (*Haase et al.* (2024a)). The mechanical properties are given in Table 2.

Table 2. Material properties (mean values).

Material		*MOE* in [N/mm²]	Bending strength f_m in [N/mm²]	Shear strength f_v in [N/mm²]	Density ρ in [kg/m³]	Moisture content in [%]
Timber	GL 24h	11,100±1400 (n = 8)	35.0±5.2	4.86±0.7	443±23	11.5±0.7
	LVL 48p	12,600±260 (n = 5)	51.7±1.3	5.99±0.2	493±5.3	9.6±0.2
	LVL 80p*	16,800*	81.7*	8.72*	841±17**	7.2±0.6**
			Yield strength f_y in [N/mm²]	Tensile strength f_u in [N/mm²]		
Steel	S355	210,000	380±15	537±14	-	-
	S420	210,000	449±20	483±0.6	-	-
			Tensile strength f_t in [N/mm²]			
Adhesive	EP1	6,300	24.6±6.8	-	-	
	EP2	5,400±110	45.0±1.4	-	-	-
	PUR	5,000±490	45.5±0.7	-	-	-

* properties derived from literature and determined from 5%-quantiles with COV = 5% and $k_s(n)$ = 1.645
** properties determined in tests

2.2 Methods

2.2.1 Specimen geometry and test programme

The tested specimens and investigated geometries are given in Figure 1.1. Geometry V was tested with mild steel S355 + GL 24h (RS − regular strength) and higher strength steel S420 + LVL 48p (HS − higher strength). Geometry V used LVL 80p for the HS combination. The area ratio of steel to timber was 10%. Table 3 gives an overview of the test campaign with composite beams under governing bending loading (4-point bending) and governing shear loading (3-point bending). The steel plates were either corundum blasted or galvanised, however, results showed no significant difference between the different surface preparations. Therefore, no further distinction was made. The naming of the specimens follows a simple code: The first letter represents the orientation of the steel sheet (V-vertical and H-horizontal). The next two letters identify the material combination (RS-regular strength and HS-higher strength). The last three letters identify the adhesive (EP1, EP2 and PUR), followed by a sequential number of the specimens in each series.

Table 3. Overview of the test campaign with number of tests for 3-point and 4-point bending setup.

Geometry	Material	3-point bending			4-point bending		
		EP1	EP2	PUR	EP1	EP2	PUR
V (vertical steel plate)	GL 24h + S355	2	2	1	2	3	1
	LVL 48p + S420	4	-	1	4	-	1
H (horizontal steel plates)	GL 24h + S355	-	-	-	2	4	1
	LVL 80p + S420	4	-	-	4	-	-

2.2.2 Manufacturing of specimens

For the manufacturing of the test specimens, all steel parts were either blasted or galvanised. Prior to bonding, the parts were degreased with methyl ethyl ketone (MEK). For the PUR adhesive, a primer was required to prepare the steel surface. The timber surface was planed within 24 hours prior to bonding. The specimens with the RS materials for the Geometry H (only for 4-point bending), were reinforced with inclined fully threaded screws ($d = 8$ mm and $\ell = 200$ mm), to increase the shear strength. The manufacturing and the reinforcement of the specimens for the 4-point bending tests is described in more detail in *Haase et al.* (2024b). The manufacture of the 3-point bending tests was analogous.

2.2.3 Experimental testing

4-point bending tests according to EN 408 (2010) were carried out on the composite beams with two different geometry and material combinations. Figure 2.1a shows the test set-up. All specimens had a height of 160 mm. To avoid local compression failure perpendicular to the grain of the wood, the load was applied directly to the steel sections via steel inlets. All specimens were tested with a span of $\ell = 2400$ mm.

In addition, 3-point bending tests, following the proposal of *Gehri* (2010), were carried out on composite beams with a much shorter span of ℓ = 740 mm, to enforce shear failure of the beams. For Geometry V, the same material combinations were tested. For Geometry H, only tests with the higher strength combination were carried out. Figure 2.1b shows the test set-up.

For comparative reasons, reference beams of GL 24h, and LVL 48p were tested with both test setups. The results were used to determine reference values (and also the material properties given in Table 2) and to highlight the performance of the various composite beams.

To evaluate the shear stiffness, the deformations of the shear fields were measured on the front of each beam with digital image correlation (DIC). With the DIC system, the displacement of the markers at the corners of the shear fields were measured. The shear stiffness *GA* was analysed for each specimen in the range of 10–40% of the ultimate load. Only the global displacement of the machine head was measured. Additionally, the steel stresses were measured using strain gauges. The location of the strain gauges was at the top and bottom fibres of the steel plate for Geometry V, and in the neutral axis of the steel plates for Geometry H. All specimens were tested with a constant loading rate of 5 mm/min. The loading was continuously increased, until failure of the beams occurred.
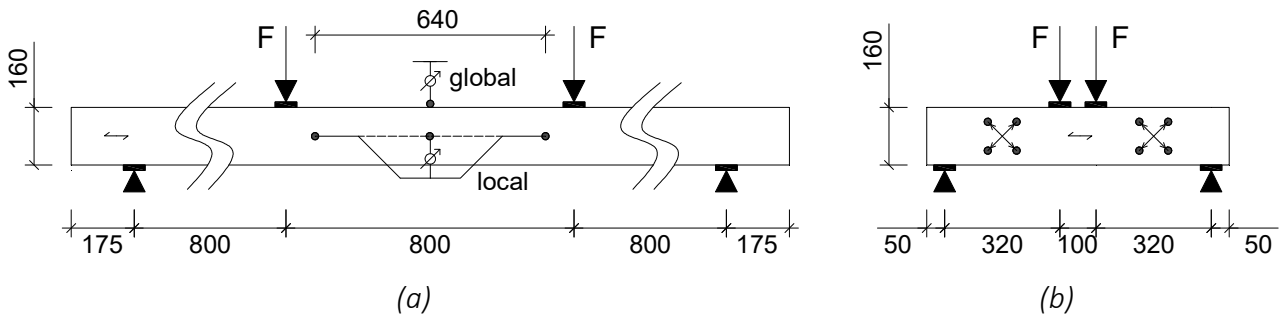

Figure 2.1. Test setup and location of measured deformations for (a) 4-point-bending tests and (b) 3-point bending tests.

2.2.4 Analytical load-carrying capacity and stiffness

Full bond between timber and steel was assumed for the analytical determination of the load-carrying capacity (as shown in *Aurand et al.* (2023)). Using the ratio of the *MOE*s of timber and steel, cross-sectional values were calculated for both steel (index S) and timber (index T). The second moment of inertia was calculated using Equation (1), and given here exemplarily related to the timber material. The bending stiffness of the composite section EI_{comp} was calculated using Equation (2):

$$I_{y,\text{rel,T}} = \sum I_{y,\text{T,i}} + \frac{E_S}{E_T} \cdot \sum I_{y,\text{S,i}} \tag{1}$$

$$EI_{comp} = E_T \cdot I_{y,\text{rel,T}} = E_S \cdot I_{y,\text{rel,S}} \tag{2}$$

The shear stresses were calculated with the first moment of inertia. Since the width of the cross-section was not constant, different locations were relevant for the evaluation of the shear stresses. For Geometry V, two locations, and Geometry H, three locations were analysed (see Figure 2.2). Since shear failure in the timber was decisive, the first moment of inertia was only analysed in relation to the timber material, see Equation (3):

$$S_{y,rel,T} = \sum S_{y,T,i} + \frac{E_S}{E_T} \cdot \sum S_{y,S,i} \quad (3)$$
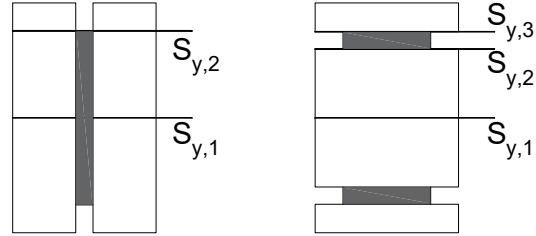
Figure 2.2. Locations for evaluating the shear stress.

The bending and shear stresses were calculated according to the mechanics of materials, using equations (4) to (6). Depending on whether the stresses were determined in the timber or in the steel, the corresponding related properties were used. With the determined mean values of the bending strength, the yield strength and the shear strength (see Table 2), the expected load-carrying capacities were calculated, using equations (7)–(9):

$$\sigma_{m,T} = \frac{M_{Ed}}{I_{y,rel,T}} \cdot z_T \quad (4)$$

$$F_{m,exp,T} = \frac{f_m \cdot I_{y,rel,T}}{a \cdot z_T} \quad (7)$$

$$\sigma_{y,S} = \frac{M_{Ed}}{I_{y,rel,S}} \cdot z_S \quad (5)$$

$$F_{y,exp,S} = \frac{f_y \cdot I_{y,rel,S}}{a \cdot z_S} \quad (8)$$

$$\tau_T = \frac{V \cdot S_{Y,i}}{I_{Y,T} \cdot \left(b_{T,i} + \frac{E_S}{E_T} \cdot b_{S,i} \right)} \quad (6)$$

$$F_{v,exp,T} = \frac{f_v \cdot I_{y,rel,T} \cdot b_i}{S_y} \quad (9)$$

3   Results and discussion

3.1   4-point-bending tests (governing bending load)

3.1.1   Geometry V (vertical steel plate)

At first, tests with vertical steel plate and the RS material combination of GL 24h and S355 were performed. Figure 3.1a shows the global load-displacement curves of all specimens. All specimens showed a very similar load-displacement behaviour, independent of the surface finish of the steel plate, and independent of the used adhesive. Therefore, they are grouped together as "vertical – regular strength" (V-RS). The average load-carrying capacity of this group was F_{max} = 75.7 kN (COV = 9.8%) (see dashed, horizontal line in Figure 3.1a). The average bending stiffness EI, evaluated in the range of 10–40% of the ultimate load, was $74.8 \cdot 10^{10}$ Nmm² (COV = 5.9%). The

average ultimate load and the average bending stiffness both correspond to an increase of 100%, compared to the GLT reference beams. This means that a reference timber beam with the same width would have to be 25% higher to achieve the same stiffness value.

The global load-displacement behaviour of all tested specimens with vertical steel plates and the material combination of LVL 48p and S420 is illustrated in Figure 3.1b. The global behaviour was very similar for all specimens with higher strength materials. Again, no significant difference was detected between the different surface conditions of the steel plate, and between the different adhesives. Therefore, all specimens are grouped as "vertical – higher strength" (V-HS). On average, the load-carrying capacity increased by 20% (compared to V-RS) to F_{max} = 91.1 kN (COV = 2.5%). The average bending stiffness EI, evaluated in the range of 10–40% of the ultimate load, is similar to the V-RS tests with $76.9 \cdot 10^{10}$ Nmm² (COV = 3.5%). The significantly lower COV confirms the homogenisation effect of the LVL in combination with the steel, which enables load redistribution into the steel, in the event of local failure of the timber. A further homogenisation of the composite beam with LVL, compared to the reference LVL beam (COV = 2.7%), was not detected. The average ultimate load corresponds to an increase of 60% and the average bending stiffness corresponds to an increase of 80%, both compared to the LVL reference beams. A reference timber beam with the same width would have to be 20% higher, to achieve the same stiffness value.
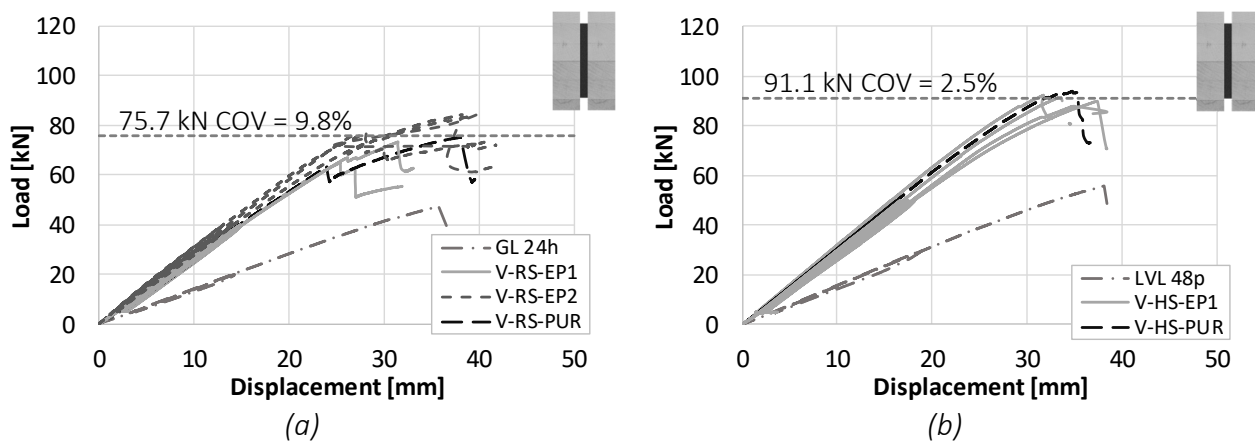

Figure 3.1. Global load-displacement curves for Geometry V: (a) GL 24h + S355 (RS) and (b) LVL 48p + S420 (HS).

3.1.2 Geometry H (horizontal steel plate)

For the regular strength specimens with GL 24h and S355, the global load-displacement behaviour is shown in Figure 3.2a. A linear load increase was observed, without any influence from the unloading loop. The specimens failed brittle due to shear failure of the timber member. Due to similar behaviour, all specimens are grouped as "horizontal – regular strength" (H-RS). On average, the ultimate load was F_{max} = 82.9 kN (COV = 12.7%), which is similar to Geometry V. However, the average bending stiffness EI, evaluated in the range of 10–40% of the ultimate load, significantly

increased to $129 \cdot 10^{10}$ Nmm² (COV = 5.5%). The failure mode of all specimens was shear failure in the timber member, which explains the larger scatter of the load-carrying capacity (as compared to Geometry V). The average ultimate load corresponds to an increase of 120% and the average bending stiffness to an increase of 250%, both compared to a GLT reference beam. A reference timber beam with the same width would have to be 50% higher, to achieve the same stiffness value.

For the timber section of the specimens with the higher strength material combination, beech LVL 80p was selected, rather than LVL 48p, because of its higher shear strength. Their global load-displacement behaviour is shown in Figure 3.2b. Here, no reinforcement screws were added to the timber member. The specimens were grouped as "horizontal – higher strength" (H-HS). As it was expected, the failure mode was shear failure in the central timber member. On average, the ultimate load increased by 44% to F_{max} = 119 kN (COV = 0.6%), compared to the RS specimens. However, the average bending stiffness EI, evaluated in the range of 10–40% of the ultimate load, did not further increase with $128 \cdot 10^{10}$ Nmm² (COV = 3.3%). The average ultimate load corresponds to an increase of 30% compared to the analytically determined load-carrying capacity of the LVL 80p. The average bending stiffness corresponds to an increase of 120%, compared to the analytical calculation. This means that a reference timber beam with the same width would have to be 30% higher, to achieve the same stiffness value.
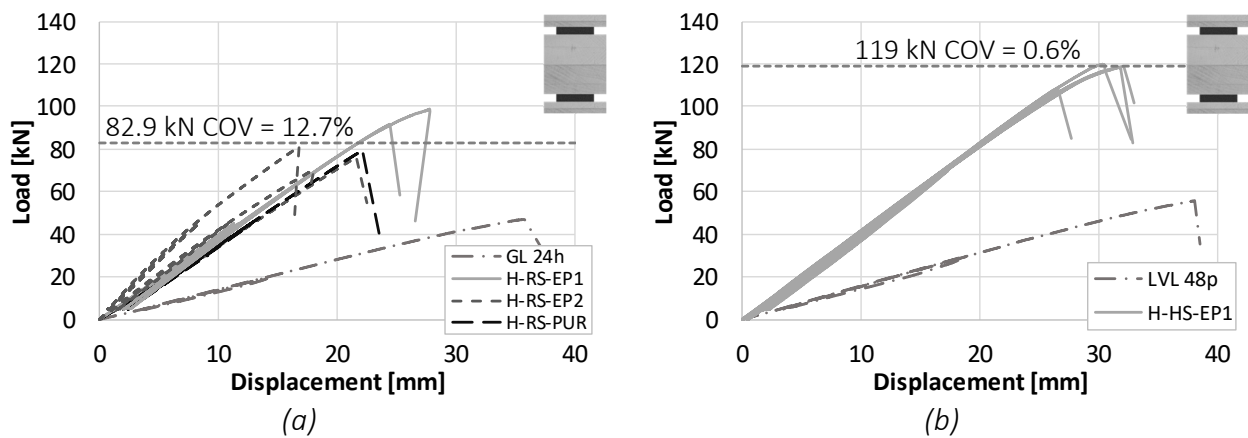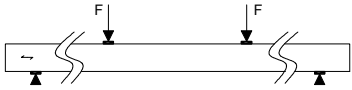

Figure 3.2. Global load-displacement curves for Geometry H: (a) GL 24h + S355 (RS) and (b) LVL 80p + S420 (HS).

The comparison of the test results to the analytical determined values shows a deviation of 14% of the expected load for H-RS. This deviation is due to the reinforcement screws in the inner timber part, which increased the shear strength.

Table 4 summarizes all results of the 4-point bending tests. In contrast to the 3-point bending tests, the span of the specimens was 2.4 m and the specimens were primarily under bending load. Additionally to the ultimate load and the bending stiffness, an equivalent bending strength f_m and an equivalent Young's modulus E were determined. Both values refer to the reference cross section of 100 x 160 mm.

Table 4. Test results of all 4-point-bending tests.

		Ultimate load F_{max} [kN]	Bending stiffness EI [$\cdot 10^{10}$ Nmm²]	Equivalent bending strength f_m [N/mm²]	Equiv. Young's modulus E [N/mm²]
Reference	GL 24h	37.3 ± 5.6	37.7 ± 4.7	35.0 ± 5.2	11,058 ± 1,370
	LVL 48p	55.1 ± 1.4	43.0 ± 0.9	51.7 ± 1.3	12,602 ± 262
	LVL 80p*/**	86.8**	57.3**	81.7*	16,800*
Vertical	GL 24h + S355	75.7 ± 7.4	74.8 ± 4.4	70.8 ± 7.0	22,000 ± 1,400
	LVL 48p + S420	91.1 ± 2.3	76.9 ± 2.7	85.4 ± 2.2	22,500 ± 800
Horizontal	GL 24h + S355	82.9 ± 10.5	129 ± 7.1	77.8 ± 2.2	37,800 ± 1,900
	LVL 80p + S420	119 ± 0.7	128 ± 4.2	112 ± 0.7	37,370 ± 1,200

* derived from literature and determined from 5%-quantile with COV = 5% and $k_s(n)$ = 1.645
** analytically determined values with derived properties of f_m and *MOE*

3.1.3 Analytical calculations

The comparison of the analytical load-carrying capacity to the test results can be seen in Figure 3.3. The minimum value of Equations (7)–(9) was the decisive, expected load-carrying capacity. For Geometry V, this was governed by the yield strength of the steel. The test results, however, showed plastic utilization of the steel profiles, exceeding the yield strength. Therefore, the deflection could be further increased, until the bending strength of the timber was reached. The tests showed bending failure of the timber and plastification of the steel, which is congruent to the analytic calculation (± 10% deviation for V-RS and V-HS). The deviation of the test results of the bending stiffness to the calculated stiffness is small with 5–8%.
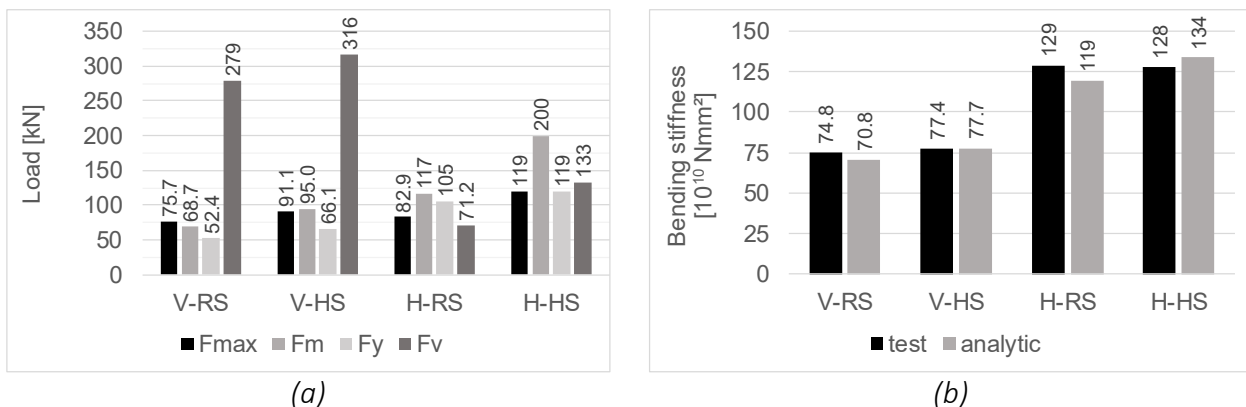

Figure 3.3. Comparison of test results to analytical results: (a) load-carrying capacity and (b) bending stiffness of 4-point bending tests.

3.2 3-point-bending tests (governing shear load)

3.2.1 Geometry V (vertical steel plate)

In this section, the results of all specimens with a vertical steel plate and the material combination of GL 24h and S355 are presented and discussed. Figure 3.4a shows the global load-displacement curves. During the tests, the deformation of the shear field and the global machine deformation were continuously measured. Therefore, all

following graphs show the displacement of the machine head. Clearly visible is some slip at the beginning of the tests. All specimens showed a very similar load-displacement behaviour, i.e. a linear increase in load and stiffness. With increasing displacement, the stiffness slightly reduces until failure occurs. The load drops by approx. 25% before remaining more or less constant as the deformation increases. Therefore, all specimens were grouped as "vertical – regular strength" (V-RS). The average load-carrying capacity of this group was F_{max} = 199 kN (COV = 5.7%). As the specimens were primarily under shear load, the shear stiffness GA was evaluated instead of the bending stiffness EI. Analogously, the shear stiffness GA was evaluated in the range of 10–40% of the ultimate load, and was on average $10.7 \cdot 10^7$ Nmm² (COV = 35%). The average ultimate load corresponds to an increase of 90%, compared to the GLT reference beams. This increase is congruent to the results from the 4-point bending tests. The average shear stiffness corresponds to an increase of 430%.

To further increase the load and stiffness, tests with a vertical steel plate and the higher strength material combination of LVL 48p and S420 were performed. The global load-displacement curves of all specimens is shown in Figure 3.4b. Again, the displayed displacement is of the machine head, which explains the visible slip at the beginning of the tests. All specimens showed a very similar load-displacement behaviour, and were, therefore, grouped as "vertical – higher strength" (V-HS). The load-displacement behaviour is similar to that of the RS specimens. The average load-carrying capacity of this group increased by 13% to F_{max} = 224 kN (COV = 3.4%). The shear stiffness GA, evaluated in the range of 10–40% of the ultimate load, was on average $7.6 \cdot 10^7$ Nmm² (COV = 39%), which is lower than for the RS specimens. But also, the shear stiffness of the LVL reference beams was lower than for the GLT reference beams. This shows that the existing differences in the shear modulus for GLT and LVL are transferred to the composite beams, and that even the use of higher strength steel cannot contribute to an increase in shear stiffness (due to the constant shear moduli of different steel grades). The average ultimate load corresponds to an increase of 75%, compared to the LVL reference beam. This is congruent to the results from the 4-point bending tests. The average shear stiffness corresponds to an increase of 380%.
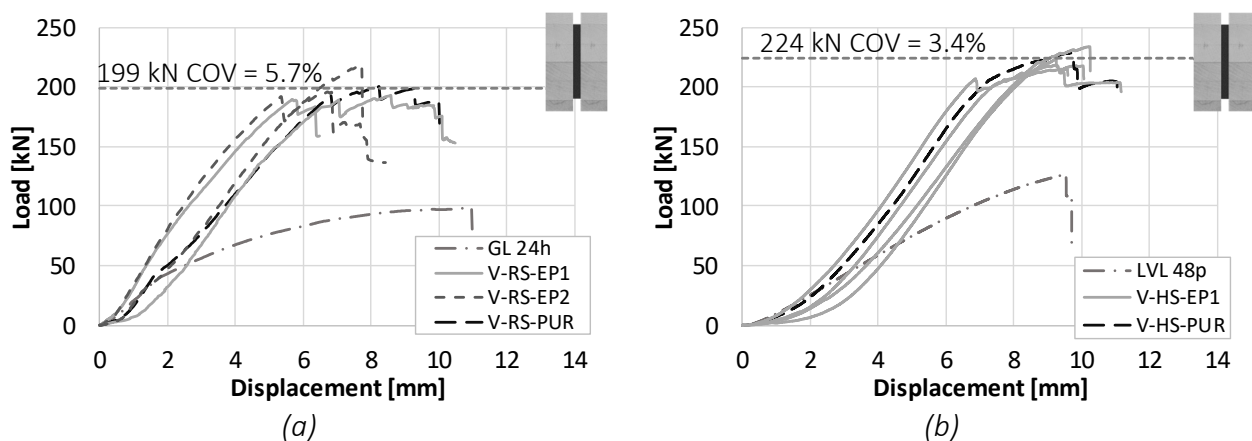

Figure 3.4. Global load-displacement (machine head) curves for Geometry V: (a) GL 24h + S355 (RS) and (b) LVL 48p + S420 (HS).

The failure of the specimens was bending-tensile failure, accompanied by secondary shear failure. Figure 3.5a shows bending-tensile failure, and Figure 3.5b+c show shear failure of a RS specimen. The bond line between steel and timber can be described as uncritical for this material combination as no failure was observed in all tests.
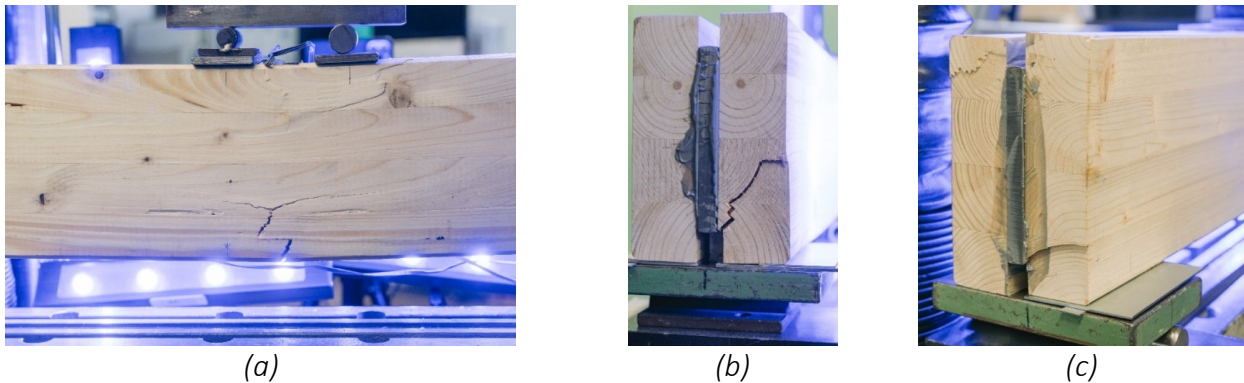

(a)   *(b)*   *(c)*

Figure 3.5. Bending tension failure (a) and shear failure of (b+c).

Figure 3.6a shows the top edge of a HS specimen. Clearly visible are kink bands that have formed in the compressive zone. This shows a full utilization of the timber section across its height. Figure 3.6b+c show secondary shear failure of the timber part that occurred with the first load drop.
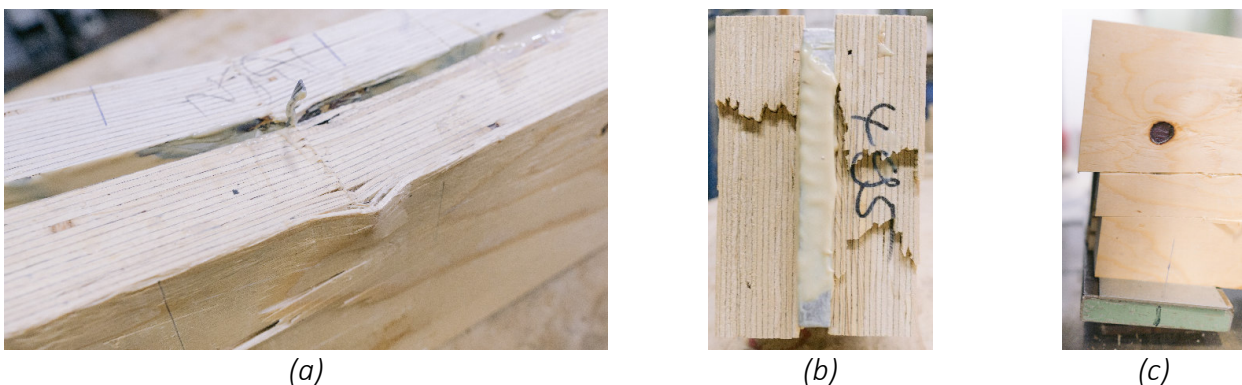

(a)   *(b)*   *(c)*

Figure 3.6. Compression kink bands at top of specimen (a) and shear failure of LVL (b+c).

After the tests, the strain gauges, attached to the edge fibres of the steel plate, were evaluated. For both material combinations, the yield strength of the steel (f_y = 380 and 448 N/mm²) was reached well before the ultimate load was achieved. This led to plastic deformation of the steel until the bending-tensile strength of the timber was reached. After brittle failure of the timber parts accompanied with a load drop, the displacement was further increased without a decrease of load-carrying capacity.

3.2.2 Geometry H (horizontal steel plate)

For the Geometry H with horizontal steel plates, only the higher strength material combination was tested, because of the predicted shear failure. Contrary to the tests before, beech LVL 80p was chosen, instead of softwood LVL. This can be explained by the higher shear strength of LVL 80p compared to LVL 48p. Timber and steel parts were bonded with the adhesive EP1. This was analogous to the 4-point bending tests. Figure 3.7a shows the load-displacement curve, with the displacement of the machine

head. Clearly visible is the large slip of one specimen at the beginning of the tests. This was assumed to result from the design of the support, where excess adhesive might have an influence. Still, all four specimens showed a very similar load-displacement behaviour, and were, therefore, grouped as "horizontal – higher strength" (V-HS). The load increases linearly up to the brittle shear failure of the specimens. The load drops by approx. 50% before it can be increased again with further displacement (shown exemplarily for one specimen in Figure 3.7a). However, the ultimate load is not reached again by any specimen. The average load-carrying capacity of all four specimens in this group, decreased to F_{max} = 167 kN (COV 2.2%). The shear stiffness GA, evaluated in the range of 10–40% of the ultimate load, was on average $2.6 \cdot 10^7$ Nmm² (COV = 5.7%). Both, the decrease in load-carrying capacity and shear stiffness (compared to Geometry V) can be explained by the failure mode of shear failure, which was completely dependent on the timber properties and not influenced by the bonded steel plates. Here, the reduced COV, especially for the shear stiffness shows the homogenized properties of the LVL. The average ultimate load shows no increase when compared to the analytically determined load-carrying capacity of a beech LVL reference beam. The average shear stiffness however, corresponds to an increase of 110%.
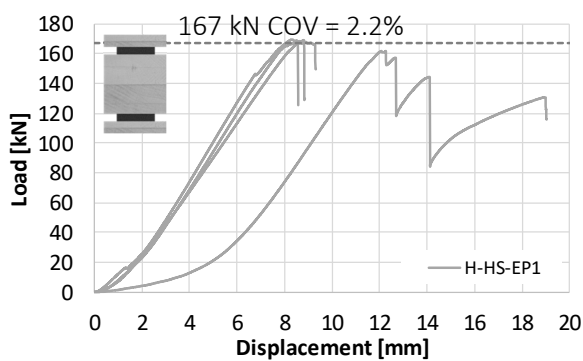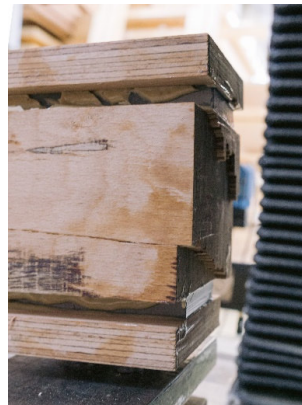
(a)   *(b)*   *(c)*

Figure 3.7. Load-displacement (machine head) curves (a) and brittel shear failure of the timber part (b+c) for Geometry H and LVL 80p + S420 (HS).

The evaluation of the strain gauges showed that the stress in the steel was at all times below the yield strength. Therefore, no plastification of the steel plates occurred. The analytical evaluation of the shear stresses across the height of the cross section (see Figure 3.8b) show shear stresses of 10.6 N/mm² (and therefore greater than the shear strength of LVL 80p) close to the bond line between the steel and the inner timber part, where the width of the specimen suddenly increases. Shear stresses of 7.50 N/mm², at half the specimen's height, were less than the shear strength of LVL 80p. That the failure occurred close to the bond line is clearly visible in Figure 3.7b+c.

Figure 3.8a shows that the analytical equations also predict the load-carrying capacity quite well for specimens primarily loaded in shear. Here, the deviation of experimental and analytical results is 6–14% for Geometry V and 20% for Geometry H.
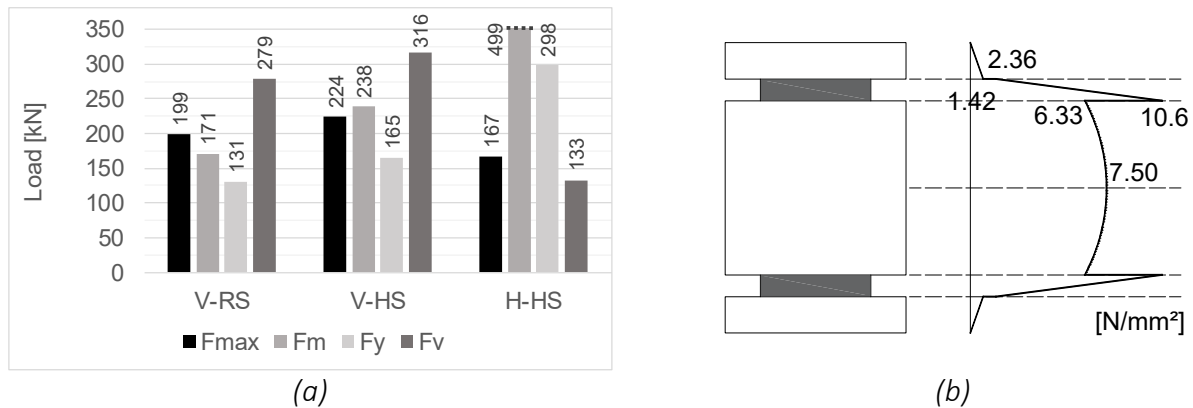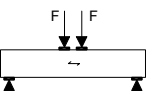

(a)   *(b)*

Figure 3.8. Comparison of test results to analytical results for 3-point bending tests (a) and shear stresses at F_{max} for Geometry H (b).

Table 5 summarizes all results of the 3-point bending tests. In contrast to the 4-point bending tests, the span of the specimens was reduced to 0.74 m and the specimens were primarily under shear load. Additionally to the ultimate load and the shear stiffness, an equivalent shear strength f_v and an equivalent shear modulus G were determined. Both values refer to the reference cross section of 100 x 160 mm.

Table 5. Test results of all 3-point-bending tests.

		Ultimate load F_{max}	Shear stiffness GA	Equivalent shear strength f_v	Equiv. shear modulus G
		[kN]	[$\cdot 10^7$ Nmm²]	[N/mm²]	[N/mm²]
Reference	GL 24h	104 ± 15	2.07 ± 0.7	4.86 ± 0.7	1,200 ± 440
	LVL 48p	128 ± 4	1.59 ± 0.2	5.99 ± 0.2	1,200 ± 140
	LVL 80p*/**	186**	1.22**	8.72*	760*
Vertical	GL 24h + S355	199 ± 11	10.7 ± 3.7	9.35 ± 0.5	6,700 ± 3100
	LVL 48p + S420	224 ± 8	7.61 ± 2.6	10.5 ± 0.4	4,700 ± 1600
Horizontal	LVL 80p + S420	167 ± 4	2.7 ± 0.2	7.83 ± 0.2	1,700 ± 120

* derived from literature and determined from 5%-quantile with COV = 5% and $k_s(n)$ = 1.645
** analytically determined values with derived properties f_v and G

4   Conclusion

The most important results are summarised below; all comparisons refer to the corresponding timber reference specimens:

- Geometry V (vertical combination) with regular-strength (RS) materials increased the load-carrying capacity by 90–100%, the bending stiffness by 100% and the shear stiffness by 430%. With higher-strength (HS) materials the load-carrying capacity was increased by 6 to 75%, the bending stiffness by 80% and the shear stiffness by

380%. Consequently, beams with Geometry V are suitable for use under high shear load.

- All specimens of Geometry V failed due to bending tensile failure in the timber part with a ductile behaviour after reaching F_{max}. The steel parts could be partially plastically utilized.

- Geometry H (horizontal combination) with regular-strength (RS) materials increased the load-carrying capacity by 120% and the bending stiffness by 250%. With higher-strength (HS) materials the load-carrying capacity was increased by up to 30%, the bending stiffness by 120% and the shear stiffness by 110%. Consequently, beams with Geometry H are suitable for use under high bending load.

- All specimens of Geometry H failed due to shear in the middle timber part. The RS material specimens could not reach the yield strength of the steel. With the HS materials, the steel was fully plastically utilised before shear failure occurred.

- For both geometry combinations, the bending and shear stiffness could not be further increased when using HS materials compared to RS materials.

- Full bond between timber and steel is confirmed by the comparison between the analytical calculations and the experimental investigations. Both the bending stiffness and the stress distribution in the cross-section could be reliably calculated analytically.

The results demonstrate the high potential of timber-steel composite beams. The geometry combination can be chosen accordingly to the governing loading mode. While the horizontal combination is ideal for structures subjected to bending loads (deflection), the vertical combination is ideal for components subjected to high shear loads. The tests have also shown that slender steel profiles, at risk of stability failure, can be used. The small deviations of test results to analytical results, however, only apply to the analysed geometry combinations. Therefore, in further numerical and experimental investigations, other material and geometry combinations must be investigated, in order to determine e.g. geometrical boundary conditions for the use of the analytical equations.

5 Acknowledgements

6   References

Alam P (2004): The reinforcement of timber for structural applications and repair [PhD thesis]. Department of Mechanical Engineering, University of Bath.

Aurand S, Boretzki J, Haase P, Ummenhofer T, Dietsch P (2023): Structural behavior of timber-steel-joints with either dowel-type fasteners or continuous joints. In: World Conference on Timber Engineering (WCTE 2023). Oslo, Norway.

Blaß HJ, Romani M (2000): Trag- und Verformungsverhalten von Verbundträgern aus Brettschichtholz und faserverstärkten Kunststoffen. Versuchsanst. für Stahl, Holz und Steine, Abt. Ingenieurholzbau, Univ. (TH): Karlsruhe.

Blaß HJ, Romani M, Schmid M (2003): Optimierung von Verbundträgern aus Brettschichtholz mit Verstärkungen aus Faserverbundkunststoffen. Versuchsanst. für Stahl, Holz und Steine, Abt. Ingenieurholzbau, Univ. (TH): Karlsruhe.

EN 408 (2010): Timber structures – Structural timber and glued laminated timber – Determination of some physical and mechanical properties. CEN: Brussels, Belgium.

EN ISO 527-2 (2012): Plastics – Determination of tensile properties – Part 2: Test conditions for moulding and extrusion plastics (ISO 527-2:2012). CEN: Brussels, Belgium.

EN ISO 6892-1 (2020): Metallic materials – Tensile testing – Part 1: Method of test at room temperature (ISO 6892-1:2019). CEN: Brussels, Belgium.

Fukutomi N, Shioya S (2018): Design method to estimate stiffness and strength of hybrid timber-steel bar beams. In: World Conference on Timber Engineering (WCTE 2018). Seoul, Korea.

Gehri E (2010): Shear problems in timber engineering – Analysis and solutions. In: World Conference on Timber Engineering (WCTE 2010). Riva del Garda, Italy.

Grunwald C, Vallée T, Fecht S, Bletz-Mühldorfer O, Diehl F, Bathon L, Myslicki S, Scholz R, Walther F (2019): Rods glued in engineered hardwood products part I: Experimental results under quasi-static loading. International Journal of Adhesion and Adhesives. 90:163–181. doi:10.1016/j.ijadhadh.2018.05.003.

Haase P, Aurand S, Boretzki J, Albiez M, Sandhaas C, Ummenhofer T, Dietsch P (2024): Bending Behavior of Hybrid Timber–Steel Beams. Materials. 17(5):1164. doi:10.3390/ma17051164.

Haase P, Boretzki J, Aurand S, Sandhaas C, Ummenhofer T, Albiez M (2024): Influence of the joining technique on the structural behaviour of hybrid timber-steel cross-sections. The Journal of Adhesion. doi:10.1080/00218464.2024.2360498.

LVL Handbook Europe (2020): 2nd ed., Federation of the Finnish Woodworking Industries: Helsinki, Finland.

Mori K, Shioya S (2021): Stiffness and strength of full-scale steel bar-timber composite beams with comparative small depth. In: World Conference on Timber Engineering (WCTE 2021). Santiago, Chile.

Riola Parada F (2016): Timber-Steel Hybrid Beams for Multi-Storey Buildings [PhD thesis]. Institut für Architekturwissenschaften, Technische Universität Wien.

Shekarchi M, Vatani Oskouei A, Raftery GM (2020): Flexural behavior of timber beams strengthened with pultruded glass fiber reinforced polymer profiles. Composite Structures. 241:112062. doi:10.1016/j.compstruct.2020.112062.